Journal of Materials Chemistry A

Chemical Switch Enabled Autonomous Two-Stage Crosslinking Polymeric Binder for High Performance Silicon Anodes

Journal:	*Journal of Materials Chemistry A*
Manuscript ID	TA-ART-08-2021-007112.R2
Article Type:	Paper
Date Submitted by the Author:	05-Nov-2021
Complete List of Authors:	Shi, Zhangxing; Argonne National Laboratory Liu, Qian; Argonne National Laboratory Yang, Zhenzhen; Argonne National Laboratory Robertson, Lily ; Argonne National Laboratory, Chemical Sciences and Engineering Division Bheemireddy, Sambasiva; Argonne National Laboratory, Electrochemical Energy Storage ZHAO, YUYUE; Argonne National Laboratory Zhang, Zhengcheng; Argonne National laboratory, Chemical Engineering Division Zhang, Lu; Argonne National Laboratory, Chemical Science & Engineering

Chemical Switch Enabled Autonomous Two-Stage Crosslinking Polymeric Binder for High Performance Silicon Anodes

*Zhangxing Shi[1], Qian Liu[1], Zhenzhen Yang,[1] Lily A. Robertson[1,2], Sambasiva R. Bheemireddy[1,2], Yuyue Zhao[1,2], Zhengcheng Zhang[1,2], and Lu Zhang[1,2]**

[1]*Chemical Sciences and Engineering Division, Argonne National Laboratory, 9700 South Cass Avenue, Lemont, IL 60439, United States*

[2]*Joint Center for Energy Storage Research, 9700 South Cass Avenue, Lemont, IL 60439, United States*

*Corresponding Author email: luzhang@anl.gov

Keywords

polymeric binder, in situ crosslinking, silicon anode, lithium-ion battery

Abstract

Silicon (Si) is a promising high-capacity anode material for high-energy-density lithium-ion batteries. However, the drastic volumetric changes of Si upon lithiation/delithiation hinder the practical use of Si anodes. Although adhesive polymeric binders, such as poly(acrylic acid) (PAA), mitigate this issue, the cycling performance of the fabricated Si anodes is still far from meeting the criteria of practical applications. Herein, we present a novel polymeric binder system for Si anodes consisting of PAA, a chemical switch (ammonia, NH_3), and a crosslinker (branched polyethylenimine, PEI). The crosslinking between PAA and PEI is switched off in slurry, which can then be turned on during electrode drying. Interestingly, the crosslinking reaction consists of two stages: ionic cross-linking (PAA-PEI-*i*) and covalent crosslinking (PAA-PEI-*c*) at a higher temperature (e.g., 130 °C). In half-cells, Si anodes fabricated using the PAA-PEI-*c* binder show a 67% increase in capacity retention compared to PAA anodes over 150 cycles at C/3 rate. The PAA-PEI-*c* binder also outperforms PAA in full cells. In addition, the chemical switch controlled crosslinking binder system also facilitates the slurry making process by avoiding early crosslinking. This system requires no additional steps compared to conventional electrode lamination process, showing enormous potential for direct adoption in large-scale manufacturing.

1. Introduction

While lithium-ion batteries (LIBs) have been recognized as the most used energy storage devices for a broad range of applications,[1] improving the energy density of LIBs is a crucial task to meet the ever-growing power demand for consumer electronics and electric vehicles.[2] The graphite-based anode materials are widely used in commercial LIBs, but they suffer from relatively low theoretical capacity (372 mAh/g based on LiC_6) limited by the crystallographic sites for storing Li ions.[2, 3] Silicon (Si), on the other hand, emerges as one of the most promising anode materials due to its impressive theoretical capacity (3579 mAh/g based on $Li_{15}Si_4$), high abundance, and low operating potential.[4-7] However, while the alloying process of Si enables accommodation of up to four Li atoms per Si atom, accounting for the extraordinary capacity, the same process also leads to dramatic volume expansions of Si upon lithiation (up to 400%).[7-9] This intrinsic feature of Si results in deleterious consequences of the fabricated electrodes, such as particle pulverization, loss of conductivity, and unstable electrode-electrolyte interfaces, consequently leading to rapid capacity loss.[10, 11] Polymers with polar functional groups have been extensively studied as binders to mitigate the undesirable behavior from Si volume changes.

The major function of binders is to provide strong adhesion/cohesion between Si particles, conductive additives, and current collector to maintain the integrity of the electrode matrix during charge/discharge processes, keeping these critical components in electronic contact for sustainable cycling performance.[12-14] In addition, polymeric binders also act as thickening agents in the electrode slurry, which facilitates the mixing process and ensures a homogeneous distribution of electrode materials.[13] The polyvinylidene fluoride (PVDF) binder has been widely utilized in graphite-based electrodes, but due to the poor adhesion and low stiffness, it fails to accommodate the drastic volume changes associated with Si.[15] Hydroxy-containing polymers such as poly(vinyl alcohol),[16] polysaccharides,[17-21] poly(acrylic acid)[22] (PAA), and polymerized cyclodextrin[23] have been demonstrated to provide promising cycling performance for Si anodes. These polymers appear to have strong binding strength possibly due to the formation of hydrogen bonding or even covalent bonding via siloxyl groups (Si-OH) that are often exist on the surface of Si particles.[13, 14, 24] Among these binders, PAA is particularly attractive due to its low cost, facile synthesis, and

excellent adhesion strength.[22, 25-27] However, the performance of PAA binder in Si electrodes still needs significant improvement in order to meet the criteria of practical applications.

Engineering PAA binders with tailored properties has been an effective approach for improving the accommodation of the Si anode, and many examples have demonstrated much improved performance by re-designing the binder systems such as incorporation of host–guest interaction,[28] copolymerization,[29] graft polymerization,[30, 31] side chain modification,[32, 33] cross-linking,[34-41] and surface coating.[42] While those examples are taking various angles, they all aim to enhance certain properties such as adhesion, cohesion, and mechanical strength of binders. Moreover, the processing conditions are another critical yet overlooked topic that dramatically impact Si anode performance.[25, 26]

Constructing a crosslinking network is effective to improve the adhesive strength and tune the mechanical properties of PAA binders.[27] The 3D network formed by crosslinking is more mechanically robust than linear polymers and firmly holds the electrode components together and improves cycle life.[41, 43] There are two types of crosslinking reactions reported to construct crosslinked networks of PAA: (1) physical crosslinking via hydrogen bonding or ionic bonding;[37, 38, 41] and (2) covalent crosslinking between PAA and small molecular[39] or polymeric crosslinkers.[34-36, 40] Although crosslinked PAA binders provide desired mechanical improvements, it is challenging to handle such materials as they are mostly either insoluble in common solvents or less processable, hindering the slurry making process of electrode fabrication or even making it impractical. Therefore, designing a crosslinking binder system for practical uses requires control of the crosslinking reactions during the slurry making process, posing challenges for implementing such a concept in real battery fabrications.

In this work, we attempt to construct an autonomous two-stage crosslinking binder system by manipulating the crosslinking processes of PAA, which enables enhanced mechanical properties in fabricated electrodes without sacrificing processability during the slurry making process. Three chemicals are involved in this system, namely PAA, ammonia (NH_3), and branched polyethylenimine (PEI). While PAA and PEI are the building block components for the crosslinking networks, NH_3 functions as both a neutralization agent to promote rheology properties

and a *chemical switch* to shut off crosslinking reactions of PAA acid groups and PEI amine groups during the slurry making process. Due to the restorable nature, this switch can be removed during electrode drying at elevated temperatures to re-enable the crosslinking between PAA and PEI after the lamination has been made.[44] Interestingly, the PAA-PEI crosslinking undergoes an autonomous two-stage process, including an ionic crosslinking (PAA-PEI-*i*) at relatively low temperature and a covalent crosslinking (PAA-PEI-*c*) at higher temperature. By fine tuning the restorable neutralization between PAA and NH_3 as well as the crosslinking between PAA and PEI, we successfully established an autonomous two-stage binder system regulated by a chemical switch and drying temperatures for Si anodes that affords much improved rheological and mechanical properties without changing slurry making process, representing an interesting and promising methodology that may lead to stable cycling of Si anodes and enormous potential for direct adoption in large-scale manufacturing.

2. Results and Discussion

Scheme 1 illustrates chemical processes of the chemical switch enabled autonomous two-stage crosslinking binder system and the role of each component at different stages, including slurry making and electrode drying. In our initial design, PAA and PEI are directly used to construct the crosslinking binder network. PEI is chosen due to its branched architecture and abundant amine groups that can effectively form ionic bonding with acids. However, while PAA and PEI are both soluble in water, upon mixing them together, precipitates form immediately (Figure S1), suggesting a crosslinked network forms through the acid-base reaction. Such immediate changes make directly using PAA and PEI as binders impossible as they need to remain soluble for slurry-based fabrication processes. To this end, we decided to introduce a recent discovered restorable neutralization agent, NH_3.[44] By adding NH_3 solution (NH_4OH) to PAA solution, the acid groups can be effectively neutralized (PAA-NH_3), inhibiting crosslinking reactions and preserving uniform solution with PEI (PAA-NH_3-PEI, Figure S1).

While NH_3 functions as a chemical switch and shuts off the crosslinking between PAA and PEI, the PAA-NH_3-PEI solution also brings in desirable rheological enhancements. The rheological properties, such as viscosity and shear thinning effects, are beneficial to slurry stability and processing.[26] Figure 1 compares the rheology behavior of the PAA-NH_3-PEI solution with that of

the PAA solution (details can be found in experimental section). PAA-NH_3-PEI solution has much enhanced viscosity compared to straight PAA solution by more than one order of magnitude at low shear rates. As the shear rate increases, the viscosity of PAA-NH_3-PEI solution decreases significantly, indicating strong shear-thinning behavior. For instance, the viscosity of PAA-NH_3-PEI solution is 7.89 Pa·s at 0.2/s, more than 30 times higher than that of PAA solution (0.25 Pa·s at 0.2/s) and decreases about 90% to 0.83 Pa·s at 1626/s. A binder solution with high viscosity can slow down sedimentation and coalescence of the suspended particles, which enhances the stability of electrode slurries.[45] The shear thinning behavior of a binder solution improves the distribution of electrode materials in the slurry by facilitating the mixing process, affording better quality of the fabricated electrode laminates.[26] In our previous report, we also compared PAA-NH_3 to the lithiated PAA (PAA-Li) binder.[44] While they both improve the rheology properties, PAA-NH_3 prevails in maintaining lower pH of the electrode slurry, affording better Si preservation and cycling performance.

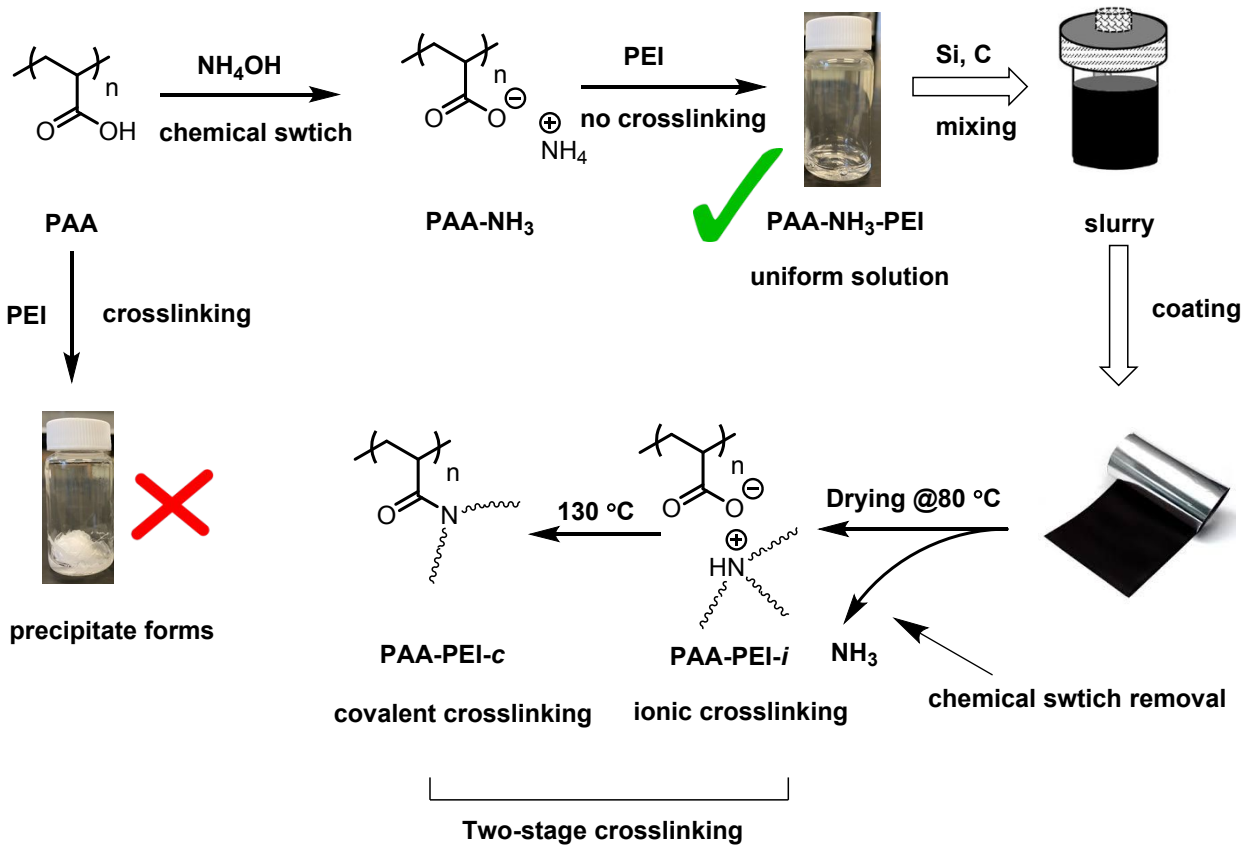

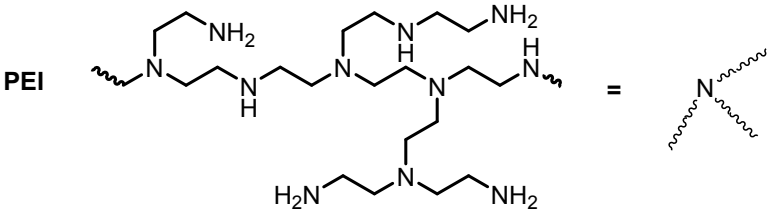

Scheme 1. Chemical processes of the two-stage crosslinking binder system.

As the solution crosslinking is inhibited by the NH_3 switch, we need to re-activate it after the lamination is completed. Fortunately, as we previously reported,[44] the ammonium carboxylate groups in PAA-NH_3 can cleave during the drying process, removing NH_3 and reactivating the crosslinking function (Scheme 1, chemical switch removal). Such a restorable process is due to the thermal instability of the ammonium salts of carboxylic acids. For instance, the analogue of the repeat unit of PAA-NH_3, ammonium acetate, can decompose to acetic acid and ammonia at 53

°C.[46] Therefore, it is reasonable to expect that PAA-NH_3 undergoes a similar thermal decomposition during the electrode dying at 80 °C or higher to regenerate PAA and re-activate the crosslinking with PEI. A detailed study of PAA-NH_3 is reported separately, confirming the restorable process is indeed occurring.[44] Although NH_3 is released during the drying process of the fabricated electrodes, the amount of NH_3 used is minimum compared to the amount of processing solvents. Compared to the widely used toxic organic processing solvent (e.g., N-methyl-2-pyrrolidone), this water-based slurry processing system is much more environmentally friendly.

Once the chemical switch (NH_3) is removed, crosslinking reactions between PAA and PEI occur. A typical crosslinking reaction between polycarboxylic acids and polyamines is via ionic bonding (i.e., physical crosslinking), which can be reversibly dissociated and recombined under certain conditions.[47] On the other hand, carboxylic acids and amines are known to directly form amides at 110 °C in the absence of catalyst,[48] and a second stage of crosslinking may take place and afford a covalent bonding network when the drying temperature is higher than 110 °C.

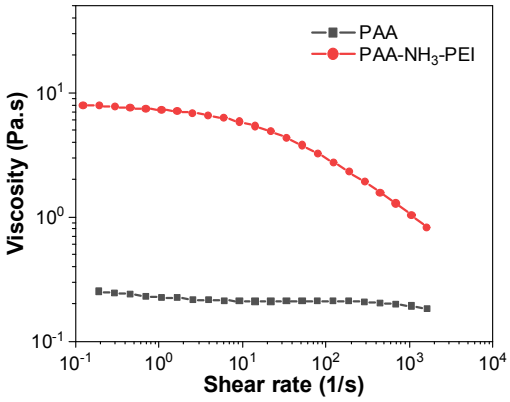

Figure 1. Plots of apparent viscosity vs. shear rate for 10 wt% aqueous solutions of PAA and PAA-NH_3-PEI.

Attenuated total reflection-Fourier transform infrared (ATR-FTIR) spectroscopy is used to monitor and validate the two-stage crosslinking processes. Figure 2 summarizes the ATR-FTIR spectra of polymer samples of PAA, PEI, PAA-PEI-*i* (dried at 80 °C) and PAA-PEI-*c* (dried at 130 °C). The carbonyl (C=O) stretching of PAA is a characteristic peak that shows at 1700 cm^{-1}

and can be observed in all samples except PEI.[26] The N-H bending peak of PEI appears at 1592 cm^{-1}.[49] A new peak at 1545 cm^{-1} was observed for PAA-PEI-*i* that is similar to the carboxylate peak of PAA-Li (1562 cm^{-1}),[26] indicating the formation of ionic crosslinking between PAA and PEI. This peak reduced significantly in PAA-PEI-*c*, while a new peak emerged at 1653 cm^{-1} as a shoulder next to the carbonyl peak. This new peak is consistent with the C=O stretching of polyamide.[50] The combination of the reduced ionic bonding and emerged covalent bonding peaks evidence the conversion of ionic crosslinking to covalent crosslinking as proposed, but the remaining ionic peaks as well as the still existing peak of carbonyl (C=O) stretching of PAA imply this conversion is not 100% and coexistence of both ionic and covalent crosslinks.

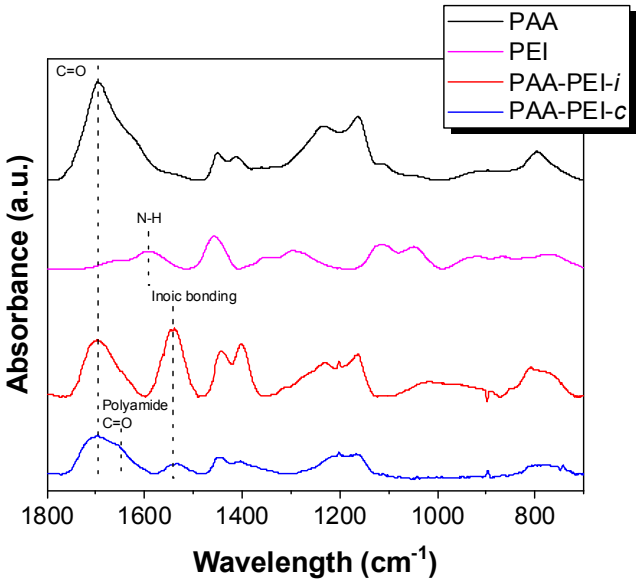

Figure 2. ATR-FTIR spectra of PAA, PEI, PAA-PEI-*i* film dried at 80 °C, and PAA-PEI-*c* film dried at 130 °C.

Solubility tests of PAA-PEI-*i* and PPA-PEI-*c* films in 1 M lithium hydroxide (LiOH) solution further show this conversion. As shown in Figure S2 in the Supporting Information, PAA-PEI-*i* film deformed immediately upon immersion in LiOH solution and almost completely dissolved after 10 min, indicating the dissociation of ionic crosslinking bonds. On the contrary, PAA-PEI-*c* film only swelled in LiOH solution and remained insoluble for at least a whole week, suggesting much better chemical resistance and a resilient crosslinking network.

While the conversion from ionic crosslinking to covalent crosslinking is not 100%, the covalent bonding really helps to strengthen the mechanical properties and even chemical stability. However, since highly crosslinked binders may not always benefit the cycling performance of silicon anode,[43] tuning the combination of ionic and covalent crosslinking may serve as a handle for further optimizations.

Peeling tests were conducted to verify the mechanical changes. Figure 3 summarizes the Load/width results of Si electrode laminates fabricated using PAA, PAA-PEI-*i* (dried at 80 °C), and PAA-PEI-*c* (dried at 130 °C) binders.[26] Details regarding the electrode fabrication and testing procedure can be found in the Experimental Section. The load/width values reflects the adhesive strength of binders used in the electrodes.[51] The average load/width value of PAA electrode (1.73 N/cm) is significantly lower than that of PAA-PEI-*i* sample (2.03 N/cm) and PAA-PEI-*c* sample (2.19 N/cm) as expected. While the enhanced adhesive strength of PAA-PEI-*i* sample can be attributed to the ionic crosslinking, the further increased cohesive strength for PAA-PEI-*c* electrode is consistent with theory of the formation of covalent crosslinking.

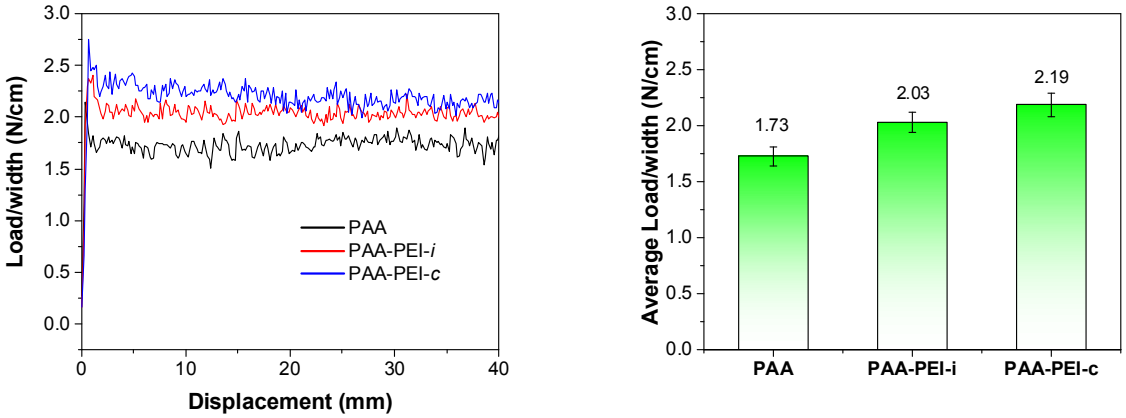

Figure 3. The 180° peeling tests for Si electrodes fabricated using PAA, PAA-PEI-*i* and PAA-PET-*c* binders (left). The averaged load/width ratios over a range of 40 mm for these electrodes (right).

The cycling performance of Si electrodes fabricated using PAA, PAA-PEI-*i* and PAA-PEI-*c* binders was evaluated in half-cells (see Experimental Section for details regarding cell assembly). Electrodes fabricated using PAA-PEI-*i* and PAA-PEI-*c* binders were dried at 80 °C and 130 °C

before cell assembly, respectively. The cells were subjected to three formation cycles between 0.01 V and 1.50 V at C/20 rate followed by 150 cycles at C/3 rate. The cycling performance of these electrodes over 150 cycles are summarized in Figure 4 (see Table S1 in Supporting Information for key parameters regarding the cycling performance). The specific capacity of each electrode was calculated based on the weight of Si particles in the electrode. As expected, the PAA electrode showed the worst overall performance with initial capacity of 2356 mAh/g and only 10% capacity retention. The PAA-PEI-*i* electrode showed a slightly lower initial capacity (2224 mAh/g) but improved capacity retention (25%). The lower initial capacity can be attributed to the pH-related side reactions of Si particles, which are commonly seen in the preparation of PAA-based electrode slurries involving a neutralization process.[26] The PAA-PEI-*c* electrode delivered similar initial capacity (2350 mAh/g) compared to that of PAA electrode, the capacity retention was dramatically improved to 77% for 150 cycles. The Coulombic efficiency (CE) also reflects the cycling performance of cells by showing capacity discrepancy between charge and discharge processes. All of the electrodes showed comparable initial CE with PAA electrode being the lowest (94.4%) and PAA-PEI-*c* electrode being the highest (95.4%). However, the CE of PAA and PAA-PEI-*i* electrodes both decreased significantly during extended cycling. Such decreases are indicative of irreversible capacity loss related to poor binding performance. The excellent capacity retention and high CE from PAA-PEI-*c* cell suggest that the dual cross-linked network indeed mitigates the issues caused by the volume changes of Si particles.

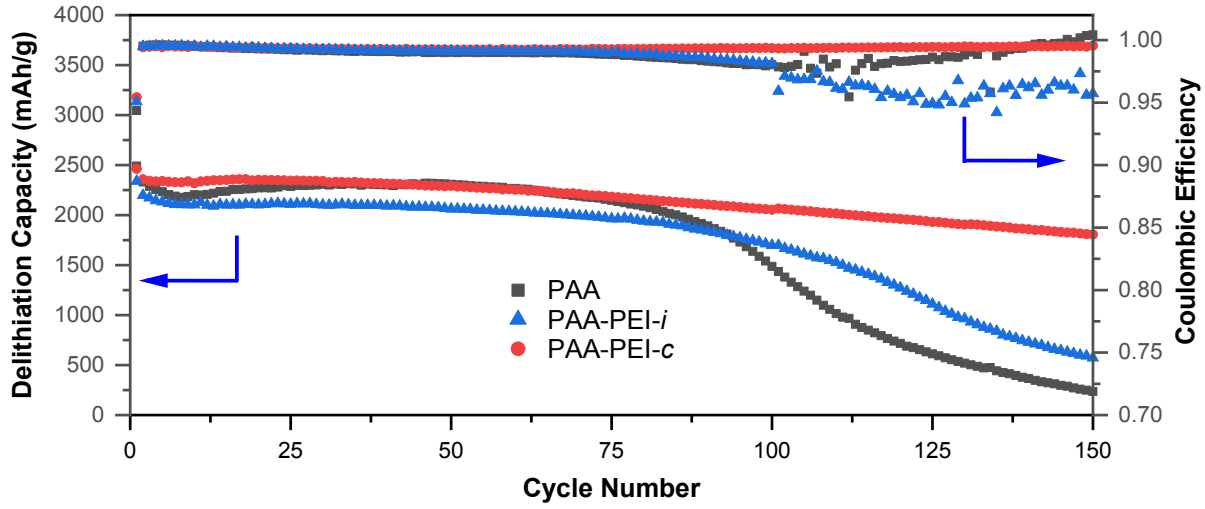

Figure 4. Cycling profiles of specific delithiation capacity (left axis) and Coulombic efficiency (right axis) of Li half-cells containing Si electrodes fabricated using PAA, PAA-PEI-*i*, and PAA-PEI-*c* binders.

The surface morphology evaluation of the fabricated Si electrodes during cycling was investigated using scanning electron microscopy (SEM). All electrodes were fully delithiated before harvested. As shown in Figure 5.1, before 150 cycles, the morphology of all electrodes looked similar and demonstrated good integrity of laminates. However, after the extended cycling, the morphology started to differ. Cracks emerged on the surface of both the PAA and PAA-PEI-*i* electrodes, while the cracking is much reduced on the latter. The PAA-PEI-*c* electrode exhibited the most preserved morphology as no noticeable changes were seen. This difference was further shown by the cross-sectional profiles. As shown Figure 5.2, the cracking after 150 cycles clearly decreased from PAA to PAA-PEI-*i* and PAA-PEI-*c*. In addition, the PAA electrode exhibits a dramatic increase in thickness (128%) after cycling, while PAA-PEI-*i* and PAA-PEI-*c* only showed 44% and 10% increase, respectively. The much better observation from PAA-PEI-*c* electrode indicates the design of dual crosslinking binders may lead to a better mitigation of the volume expansion issue of Si anodes.

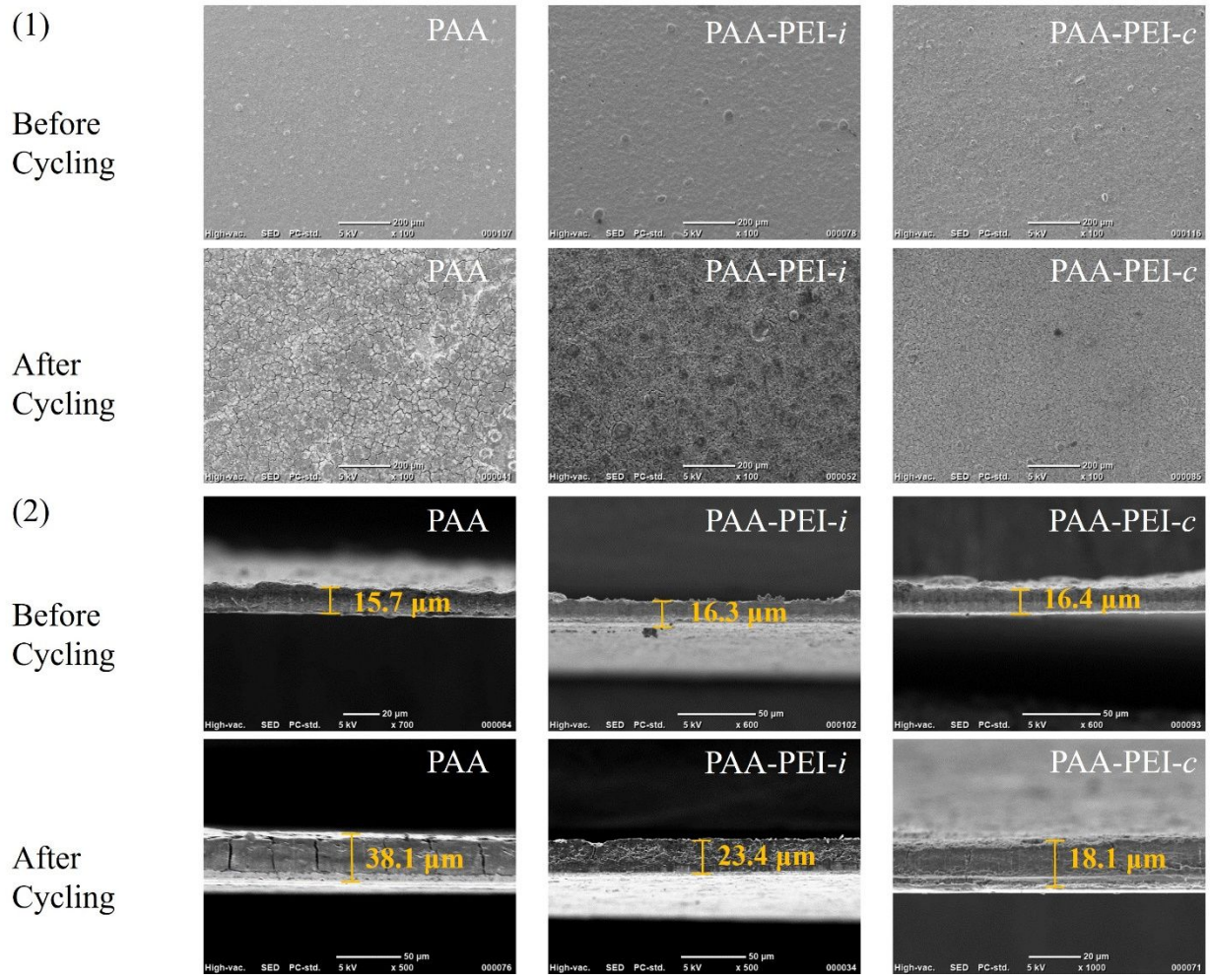

Figure 5. (1) Surface SEM images of Si electrodes fabricated using PAA, PAA-PEI-*i*, or PAA-PEI-*c* binder before and after 150 cycles (100 times magnification). (2) Cross-sectional SEM images of these electrodes before and after 150 cycles (500 to 700 times magnification except PAA-PEI-*c* after cycle at 1000 times magnification).

The surface evolution of the cycled Si electrodes fabricated using PAA or PAA-PEI-*c* binder was investigated using X-ray photoelectron spectroscopy (XPS). Figure 6 shows the F 1s and Si 2p spectra of the fabricated Si electrodes after 150 cycles (see Figure S3 for the C 1s, Li 1s, and P 2p XPS spectra). Both the PAA and PAA-PEI-*c* electrodes show the presence of LiF and P-F ($Li_xPO_yF_z$) bonds. However, the LiF content in PAA-PEI-*c* electrode is higher than that of PAA electrode. LiF is considered as a critical component for robust SEI on Si anode.[52] In addition, PAA electrode shows no obvious peaks in Si 2p spectrum. On the contrary, PAA-PEI-*c* electrode shows the peaks of Si^0 and Si^{4+} (Li_xSiO_y), indicating a thinner SEI was formed on PAA-PEI-*c* electrode

and the Si particles were better preserved in PAA-PEI-*c* electrode after extended cycling. The N content was below the testing limit of our instrument, implying the PAA-PEI-*c* binder may not be present in the SEI.

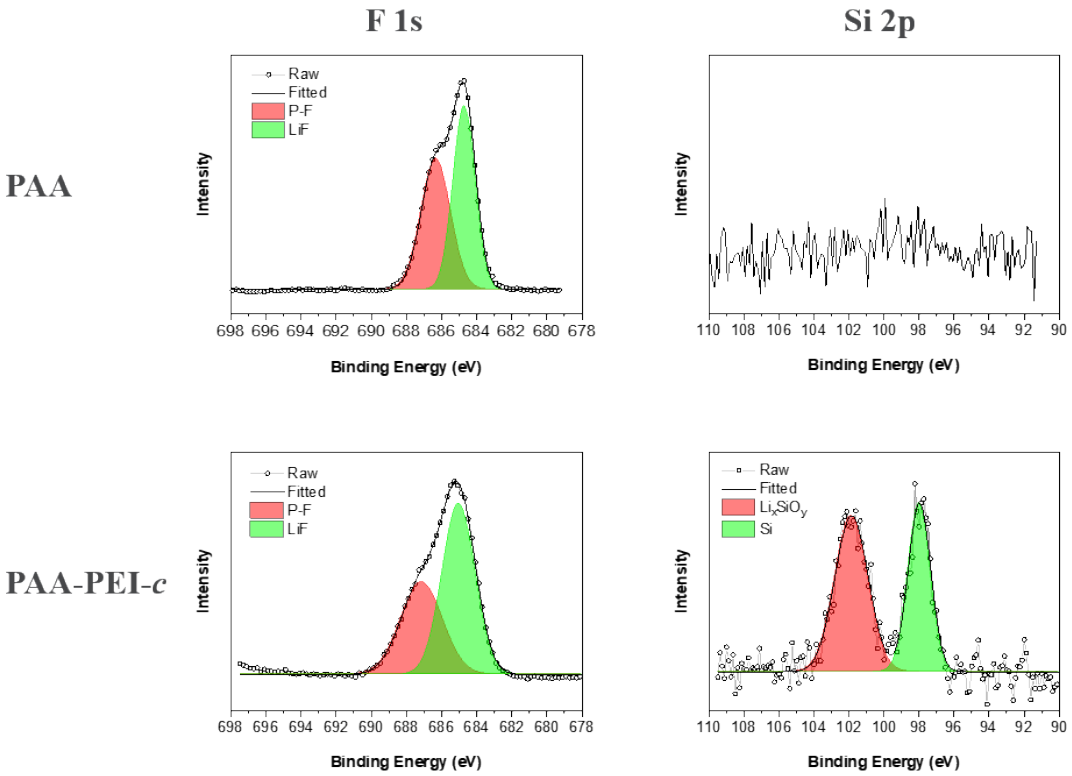

Figure 6. F 1s and Si 2p XPS spectra of the PAA and PAA-PEI-*c* electrodes after 150 cycles.

Finally, the best-performing binder, PAA-PEI-*c* was evaluated in full cells by pairing Si electrodes with $LiNi_{0.6}Mn_{0.2}Co_{0.2}O_2$ (NMC622) cathodes. The full cells were cycled between 3.0 V and 4.2 V using a standard cycling protocol including three formation cycles at C/20 rate, a Hybrid Pulse Power Characterization (HPPC), 92 cycles at C/3 rate, another HPPC, and finally three cycles at C/20 rate. The specific discharge capacity, Coulombic efficiency (CE), and area specific impedance (ASI) results are summarized in Figure 7. More details regarding the cycling measures are summarized in Table S2 in Supporting Information. As expected, the PAA-PEI-*c* cell outperformed PAA cell by delivering higher average capacity, CE, and capacity retention. For instance, the PAA-PEI-*c* cell delivered a 73% capacity retention that is 14% improved compared to PAA cell (59%). While both cells showed comparable capacities at the beginning of C/3 cycling, the capacity of the PAA cell decreased at a much faster rate as the cycling continued. The results

are consistent with the ones from half-cells, further convincing the superior performance of the PAA-PEI-*c* binder. As for the ASI data, both cells showed almost identical values before C/3 cycling. However, the impedance of PAA cell increased significantly more than that of PAA-PEI-*c* cell after extended cycling, implying a more stable interface between the electrode and electrolyte in the PAA-PEI-*c* cell.

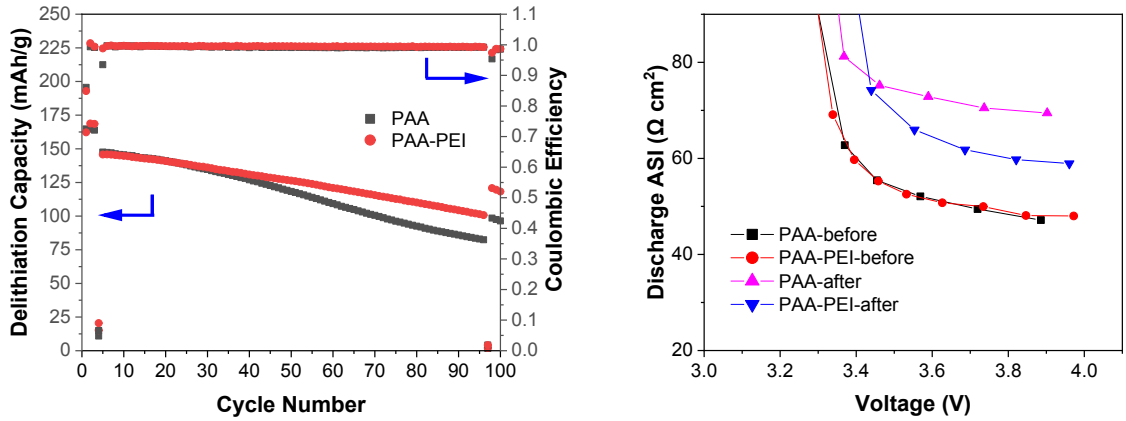

Figure 7. The capacity and Coulombic efficiency profiles (left) and HPPC results (right) of PAA and PAA-PEI-*c* full cells.

3. Conclusion

In this study, we developed a novel chemical switch enabled autonomous two stage crosslinking polymeric binder system that not only enhances the electrode integrity by bringing in crosslinking architecture of the polymer binders but also bypasses the difficulty of the laminating processing by chemically switching off the crosslinking during the slurry making process. Three components were carefully introduced, including PAA as the backbone binder, NH_3 as the chemical switch, and branched PEI as the crosslinker. PAA was firstly neutralized by the addition of NH_3, which not only improved the rheology of the binder solutions by forming the ionic PAA-NH_3 but also switched off the ionic crosslinking reaction between PAA and PEI. This switch can be removed during electrode drying as carboxylate ammonium bonds undergo a thermal decomposition to restore the acid groups, leading to *in situ* crosslinking between PAA and PEI. Interestingly, the crosslinking reaction of PAA and PEI is temperature dependent and consists of two stages: ionic cross-linking of PAA-PEI-*i* and covalent crosslinking of PAA-PEI-*c* triggered by temperature higher than 110 °C. By fully characterizing the PAA-PEI-*i* and PAA-PEI-*c* binders and electrodes,

we observe very different properties, including chemical resistance, mechanical resilience, and binding strength. Si anodes fabricated using the PAA-PEI-*c* binder (electrodes were dried at 130 °C) delivered much improved cycling performance. The PAA-PEI-*c* half-cell shows 77% capacity retention over 150 cycles at C/3 rate, affording a 67% increase compared to that of PAA half-cell. In full cells, the PAA-PEI-*c* cell also outperforms the PAA cell in terms of average capacity, Coulombic efficiency, capacity retention, and impedance. By elegantly utilizing the restoration feature of PAA-NH_3 and thermal triggered crosslinking reactions between PAA and PEI, we developed a novel two stage autonomous crosslinking binder system, PAA-PEI-*c,* that not only dramatically improves cycling performance of the fabricated Si anodes but also facilitates the slurry making process by avoiding early crosslinking. This carefully designed system controls the property enhancing crosslinking reactions over the whole electrode fabrication process and requires no additional steps compared to conventional electrode lamination process, demonstrating enormous potential for direct adoption in large-scale manufacturing of Si electrodes.

4. Experimental Section

Materials

Poly(acrylic acid) (PAA, M_n = 130,000), branched polyethylenimine (PEI, M_n = 10,000), lithium hydroxide, and ammonium hydroxide solution (28% ammonia in water) were purchased from Sigma-Aldrich. Silicon nanoparticles (150 nm) were purchased from Paraclete Energy, Inc. Conductive carbon particles (C45, 50–60 nm) were purchased from Timcal. The fabricated Si electrodes contain 70 wt% silicon, 20 wt% binder, and 10 wt% C45. NMC622 positive electrodes that contain 90 wt% $LiNi_{0.6}Mn_{0.2}Co_{0.2}O_2$, 5 wt% C45, and 5 wt% PVDF binder were produced by the Cell Analysis, Modeling, and Prototyping (CAMP) facility of Argonne National Laboratory. Gen 2 electrolyte (1.2 M $LiPF_6$ in ethylene carbonate and ethyl methyl carbonate with weight ratio of 3:7) was purchased from Tomiyama Pure Chemical Industries. Fluoroethylene carbonate (FEC) was purchased from Solvay, dried, and distilled before use.

Preparation of PAA-NH_3-PEI solution

PAA (1.0 g) and deionized water (8.0 g) were added to a 50 mL round bottom flask equipped with a magnetic stir bar. Ammonium hydroxide solution (1.0 g) was then added to neutralize PAA. After stirring at room temperature for 2 h, PEI solution (0.1 g, 10 wt% PEI in deionized water)

was added dropwise. The resulting mixture was stirred at room temperature for 8 h to yield a homogenous PAA-NH_3-PEI solution. The weight ratio between PAA and PEI is 100:1 in the PAA-NH_3-PEI solution.

Rheological Measurements

Rheological characterization of binder solutions was conducted at 25 °C using a TA Instruments model Discovery HR-3 rheometer equipped with a cone-plate geometry that has a cone diameter of 20 mm and an angle of 2° (truncation 52 μm). To minimize water evaporation, a solvent trap cover was used during the tests. The apparent viscosity at different shear rates was measured in a flow ramp.

Attenuated Total Reflection-Fourier Transform Infrared (ATR-FTIR) Spectroscopy

ATR-FTIR spectra of binder samples were collected using a PerkinElmer Spectrum 100 FT-IR Spectrometer equipped with a universal ATR sampling accessory.

Peeling Tests

Peeling tests of Si electrodes were conducted using an Instron 3343 universal tester to evaluate the adhesive strength of the binders. The laminate side of the electrode (30 mm × 90 mm) was attached to 3M 600 Scotch tape (1 inch in width). The electrode was peeled by pulling the tape at an angle of 180° and a constant displacement rate of 20 mm/min. The applied force was measured to produce the load/width vs displacement plots.

Cell Assembly and Electrochemical Characterization

The Si electrode laminates were coated on a copper foil current collector using a doctor blade from a thoroughly mixed electrode slurry containing 70 wt% Si nanoparticles, 20 wt% binder, and 10 wt% C45. The fabricated electrodes were dried at 80 °C for 12 h, calendared, punched into 1.5 cm^2 disks, and further dried in a vacuum oven at 80 °C or 130 °C for 8 h before assembling into 2032-type stainless steel coin cells. For half-cell evaluation, the cells were configured with a lithium metal counter electrode, a microporous polypropylene separator (Celgard 2325), a Si electrode, and Gen 2 electrolyte containing 10 wt% FEC (25 μL). The cells were subjected to three formation cycles at C/20 rate followed by 150 cycles at C/3 rate with the voltage window between

0.01 and 1.5 V. The electrochemical performance of each binder was determined by the average of two parallel cells. The fabricated electrodes show excellent reproducible cycling performance among different batches (see Figure S4 in Supporting Information). For full cell evaluation, the Si anodes were paired with NMC622 cathodes with a N/P ratio of 1.1. The cycling voltage was maintained between 3.0 V and 4.2 V with a cell testing protocol consisting of (i) three formation cycles at C/20 rate, (ii) a hybrid pulse power characterization (HPPC) sequence to measure area specific impedance (ASI) at different depths of discharge (DOD), (iii) 92 cycles at C/3 rate, (iv) another HPPC sequence, and (v) three final cycles at C/20 rate to measure capacity retention. In the HPPC test, the cells were charged at C/3 rate to 4.2 V, discharged at C/3 rate to 10% DOD, rested at the open circuit voltage for 1 h, and then subjected to hybrid pulse sequence. The hybrid pulse sequence includes a discharge pulse at 3C rate for 10 s, a rest for 40 s, a charge pulse at 2.25C rate for 10 s, and another rest for 60 s. The impedance was calculated by using the applied current and the voltage differences before and after pulses.

Scanning Electron Microscope (SEM) Measurements

The cycled coin cells were disassembled in an argon-filled glovebox. The harvested Si electrodes were rinsed with anhydrous dimethyl carbonate and dried. The surface morphology and cross-sectional thickness of the pristine and cycled electrodes were investigated using a JEOL JCM-6000Plus scanning electron microscope (SEM).

X-ray photoelectron spectroscopy (XPS)

The Si anodes after cycling was washed with DMC and dried before moving to the XPS chamber. XPS data were acquired using PHI 5000 VersaProbe II system (Physical Electronics) that attached to an argon-atmosphere glovebox to avoid any contamination of moisture and air. The X-ray source was operating at 25 W equipped with monochromatic Al Kα radiation (hυ = 1486.6 eV) which was set at Ar+-ion and electron beam sample neutralization, fixed analyzer transmission mode. The base pressure in the XPS chamber was $\sim 1 \times 10^{-8}$ torr. The spectra of all samples were collected at a pass energy of 23.50 eV and electron escape angle of 45° to the sample plane. The spot size for X-ray beam was set to 100 μm. C-C peak at 284.8 eV was used to calibrate the spectra. The Shirly background data were subjected from all spectra.

Supporting Information

Acknowledgements

This research is supported by the U. S. Department of Energy, Vehicle Technologies Office (DOE-VTO). The submitted manuscript has been created by UChicago Argonne, LLC, operator of Argonne National Laboratory ("Argonne"). Argonne, a U.S. Department of Energy Office of Science laboratory, is operated under Contract No. DE-AC02-06CH11357. The U.S. Government retains for itself, and others acting on its behalf, a paid-up nonexclusive, irrevocable worldwide license in said article to reproduce, prepare derivative works, distribute copies to the public, and perform publicly and display publicly, by or on behalf of the Government. Use of the Center for Nanoscale Materials, an Office of Science user facility, was supported by the U.S. Department of Energy, Office of Science, Office of Basic Energy Sciences, under Contract No. DE-AC02-06CH11357. We would like to thank the Cell Analysis, Modeling, and Prototyping (CAMP) facility of Argonne for proving the electrode materials.

Conflict of Interest

The authors declare no conflict of interest.

References

1. Blomgren, G. E., The Development and Future of Lithium Ion Batteries. *Journal of The Electrochemical Society* **2016,** *164* (1), A5019-A5025.
2. Choi, J. W.; Aurbach, D., Promise and Reality of Post-Lithium-Ion Batteries with High Energy Densities. *Nature Reviews Materials* **2016,** *1* (4), 16013.
3. Tarascon, J. M.; Armand, M., Issues and Challenges Facing Rechargeable Lithium Batteries. *Nature* **2001,** *414* (6861), 359-367.
4. Obrovac, M. N.; Krause, L. J., Reversible Cycling of Crystalline Silicon Powder. *Journal of The Electrochemical Society* **2007,** *154* (2), A103-A108.
5. Park, C.-M.; Kim, J.-H.; Kim, H.; Sohn, H.-J., Li-Alloy Based Anode Materials for Li Secondary Batteries. *Chemical Society Reviews* **2010,** *39* (8), 3115-3141.
6. Feng, K.; Li, M.; Liu, W.; Kashkooli, A. G.; Xiao, X.; Cai, M.; Chen, Z., Silicon-Based Anodes for Lithium-Ion Batteries: From Fundamentals to Practical Applications. *Small* **2018,** *14* (8), 1702737.
7. Zhu, B.; Wang, X.; Yao, P.; Li, J.; Zhu, J., Towards High Energy Density Lithium Battery Anodes: Silicon and Lithium. *Chemical Science* **2019,** *10* (30), 7132-7148.

8. Obrovac, M. N.; Christensen, L., Structural Changes in Silicon Anodes during Lithium Insertion/Extraction. *Electrochemical and Solid-State Letters* **2004,** *7* (5), A93-A96.
9. Beaulieu, L. Y.; Eberman, K. W.; Turner, R. L.; Krause, L. J.; Dahn, J. R., Colossal Reversible Volume Changes in Lithium Alloys. *Electrochemical and Solid-State Letters* **2001,** *4* (9), A137-A140.
10. Wu, H.; Cui, Y., Designing Nanostructured Si Anodes for High Energy Lithium Ion Batteries. *Nano Today* **2012,** *7* (5), 414-429.
11. Chae, S.; Ko, M.; Kim, K.; Ahn, K.; Cho, J., Confronting Issues of the Practical Implementation of Si Anode in High-Energy Lithium-Ion Batteries. *Joule* **2017,** *1* (1), 47-60.
12. Nguyen, C. C.; Yoon, T.; Seo, D. M.; Guduru, P.; Lucht, B. L., Systematic Investigation of Binders for Silicon Anodes: Interactions of Binder with Silicon Particles and Electrolytes and Effects of Binders on Solid Electrolyte Interphase Formation. *ACS Applied Materials & Interfaces* **2016,** *8* (19), 12211-12220.
13. Chen, H.; Ling, M.; Hencz, L.; Ling, H. Y.; Li, G.; Lin, Z.; Liu, G.; Zhang, S., Exploring Chemical, Mechanical, and Electrical Functionalities of Binders for Advanced Energy-Storage Devices. *Chemical Reviews* **2018,** *118* (18), 8936-8982.
14. Kwon, T.-w.; Choi, J. W.; Coskun, A., The Emerging Era of Supramolecular Polymeric Binders in Silicon Anodes. *Chemical Society Reviews* **2018,** *47* (6), 2145-2164.
15. Farooq, U.; Choi, J.-H.; Atif Pervez, S.; Yaqub, A.; Kim, D.-H.; Lee, Y.-J.; Saleem, M.; Doh, C.-H., Effect of Binder and Composition Ratio on Electrochemical Performance of Silicon/Graphite Composite Battery Electrode. *Materials Letters* **2014,** *136*, 254-257.
16. Park, H.-K.; Kong, B.-S.; Oh, E.-S., Effect of High Adhesive Polyvinyl Alcohol Binder on the Anodes of Lithium Ion Batteries. *Electrochemistry Communications* **2011,** *13* (10), 1051-1053.
17. Li, J.; Lewis, R. B.; Dahn, J. R., Sodium Carboxymethyl Cellulose. *Electrochemical and Solid-State Letters* **2007,** *10* (2), A17-A20.
18. Kovalenko, I.; Zdyrko, B.; Magasinski, A.; Hertzberg, B.; Milicev, Z.; Burtovyy, R.; Luzinov, I.; Yushin, G., A Major Constituent of Brown Algae for Use in High-Capacity Li-Ion Batteries. *Science* **2011,** *334* (6052), 75-79.
19. Jeong, Y. K.; Kwon, T.-w.; Lee, I.; Kim, T.-S.; Coskun, A.; Choi, J. W., Millipede-Inspired Structural Design Principle for High Performance Polysaccharide Binders in Silicon Anodes. *Energy & Environmental Science* **2015,** *8* (4), 1224-1230.
20. Ling, M.; Xu, Y.; Zhao, H.; Gu, X.; Qiu, J.; Li, S.; Wu, M.; Song, X.; Yan, C.; Liu, G.; Zhang, S., Dual-Functional Gum Arabic Binder for Silicon Anodes in Lithium Ion Batteries. *Nano Energy* **2015,** *12*, 178-185.
21. Guo, S.; Li, H.; Li, Y.; Han, Y.; Chen, K.; Xu, G.; Zhu, Y.; Hu, X., SiO2-Enhanced Structural Stability and Strong Adhesion with a New Binder of Konjac Glucomannan Enables Stable Cycling of Silicon Anodes for Lithium-Ion Batteries. *Advanced Energy Materials* **2018,** *8* (24), 1800434.
22. Magasinski, A.; Zdyrko, B.; Kovalenko, I.; Hertzberg, B.; Burtovyy, R.; Huebner, C. F.; Fuller, T. F.; Luzinov, I.; Yushin, G., Toward Efficient Binders for Li-Ion Battery Si-Based Anodes: Polyacrylic Acid. *ACS Applied Materials & Interfaces* **2010,** *2* (11), 3004-3010.
23. Jeong, Y. K.; Kwon, T.-w.; Lee, I.; Kim, T.-S.; Coskun, A.; Choi, J. W., Hyperbranched β-Cyclodextrin Polymer as an Effective Multidimensional Binder for Silicon Anodes in Lithium Rechargeable Batteries. *Nano Letters* **2014,** *14* (2), 864-870.
24. Bridel, J. S.; Azaïs, T.; Morcrette, M.; Tarascon, J. M.; Larcher, D., In Situ Observation and Long-Term Reactivity of Si/C/CMC Composites Electrodes for Li-Ion Batteries. *Journal of The Electrochemical Society* **2011,** *158* (6), A750-A759.
25. Hu, B.; Shkrob, I. A.; Zhang, S.; Zhang, L.; Zhang, J.; Li, Y.; Liao, C.; Zhang, Z.; Lu, W.; Zhang, L., The Existence of Optimal Molecular Weight for Poly(acrylic acid) Binders in Silicon/Graphite Composite Anode for Lithium-Ion Batteries. *Journal of Power Sources* **2018,** *378*, 671-676.

26. Hu, B.; Jiang, S.; Shkrob, I. A.; Zhang, J.; Trask, S. E.; Polzin, B. J.; Jansen, A.; Chen, W.; Liao, C.; Zhang, Z.; Zhang, L., Understanding of Pre-Lithiation of Poly(acrylic acid) Binder: Striking the Balances Between the Cycling Performance and Slurry Stability for Silicon-Graphite Composite Electrodes in Li-Ion Batteries. *Journal of Power Sources* **2019,** *416*, 125-131.
27. Jiang, S.; Hu, B.; Shi, Z.; Chen, W.; Zhang, Z.; Zhang, L., Re-Engineering Poly(Acrylic Acid) Binder toward Optimized Electrochemical Performance for Silicon Lithium-Ion Batteries: Branching Architecture Leads to Balanced Properties of Polymeric Binders. *Advanced Functional Materials* **2020,** *30* (10), 1908558.
28. Choi, S.; Kwon, T.-w.; Coskun, A.; Choi, J. W., Highly Elastic Binders Integrating Polyrotaxanes for Silicon Microparticle Anodes in Lithium Ion Batteries. *Science* **2017,** *357* (6348), 279-283.
29. Jeena, M. T.; Lee, J.-I.; Kim, S. H.; Kim, C.; Kim, J.-Y.; Park, S.; Ryu, J.-H., Multifunctional Molecular Design as an Efficient Polymeric Binder for Silicon Anodes in Lithium-Ion Batteries. *ACS Applied Materials & Interfaces* **2014,** *6* (20), 18001-18007.
30. He, J.; Zhang, L., Polyvinyl Alcohol Grafted Poly (acrylic acid) as Water-Soluble Binder with Enhanced Adhesion Capability and Electrochemical Performances for Si Anode. *Journal of Alloys and Compounds* **2018,** *763*, 228-240.
31. Gao, Y.; Qiu, X.; Wang, X.; Gu, A.; Zhang, L.; Chen, X.; Li, J.; Yu, Z., Chitosan-g-Poly(acrylic acid) Copolymer and Its Sodium Salt as Stabilized Aqueous Binders for Silicon Anodes in Lithium-Ion Batteries. *ACS Sustainable Chemistry & Engineering* **2019,** *7* (19), 16274-16283.
32. Park, Y.; Lee, S.; Kim, S.-H.; Jang, B. Y.; Kim, J. S.; Oh, S. M.; Kim, J.-Y.; Choi, N.-S.; Lee, K. T.; Kim, B.-S., A Photo-Cross-Linkable Polymeric Binder for Silicon Anodes in Lithium Ion Batteries. *RSC Advances* **2013,** *3* (31), 12625-12630.
33. Li, J.; Zhang, G.; Yang, Y.; Yao, D.; Lei, Z.; Li, S.; Deng, Y.; Wang, C., Glycinamide Modified Polyacrylic Acid as High-Performance Binder for Silicon Anodes in Lithium-Ion Batteries. *Journal of Power Sources* **2018,** *406*, 102-109.
34. Koo, B.; Kim, H.; Cho, Y.; Lee, K. T.; Choi, N.-S.; Cho, J., A Highly Cross-Linked Polymeric Binder for High-Performance Silicon Negative Electrodes in Lithium Ion Batteries. *Angewandte Chemie International Edition* **2012,** *51* (35), 8762-8767.
35. Song, J.; Zhou, M.; Yi, R.; Xu, T.; Gordin, M. L.; Tang, D.; Yu, Z.; Regula, M.; Wang, D., Interpenetrated Gel Polymer Binder for High-Performance Silicon Anodes in Lithium-ion Batteries. *Advanced Functional Materials* **2014,** *24* (37), 5904-5910.
36. Hwang, C.; Joo, S.; Kang, N.-R.; Lee, U.; Kim, T.-H.; Jeon, Y.; Kim, J.; Kim, Y.-J.; Kim, J.-Y.; Kwak, S.-K.; Song, H.-K., Breathing Silicon Anodes for Durable High-Power Operations. *Scientific Reports* **2015,** *5* (1), 14433.
37. Lee, K.; Lim, S.; Tron, A.; Mun, J.; Kim, Y.-J.; Yim, T.; Kim, T.-H., Polymeric Binder Based on PAA and Conductive PANI for High Performance Silicon-Based Anodes. *RSC Advances* **2016,** *6* (103), 101622-101625.
38. Lim, S.; Lee, K.; Shin, I.; Tron, A.; Mun, J.; Yim, T.; Kim, T.-H., Physically Cross-Linked Polymer Binder Based on Poly(acrylic acid) and Ion-Conducting Poly(ethylene glycol-co-benzimidazole) for Silicon Anodes. *Journal of Power Sources* **2017,** *360*, 585-592.
39. Zeng, X.; Shi, Y.; Zhang, Y.; Tang, R.; Wei, L., Vinyltriethoxysilane Crosslinked Poly(acrylic acid sodium) as a Polymeric Binder for High Performance Silicon Anodes in Lithium Ion Batteries. *RSC Advances* **2018,** *8* (51), 29230-29236.
40. Xu, Z.; Yang, J.; Zhang, T.; Nuli, Y.; Wang, J.; Hirano, S.-i., Silicon Microparticle Anodes with Self-Healing Multiple Network Binder. *Joule* **2018,** *2* (5), 950-961.
41. Zhu, L.; Du, F.; Zhuang, Y.; Dai, H.; Cao, H.; Adkins, J.; Zhou, Q.; Zheng, J., Effect of Crosslinking Binders on Li-Storage Behavior of Silicon Particles as Anodes for Lithium Ion Batteries. *Journal of Electroanalytical Chemistry* **2019,** *845*, 22-30.

42. Bie, Y.; Yang, J.; Liu, X.; Wang, J.; Nuli, Y.; Lu, W., Polydopamine Wrapping Silicon Cross-linked with Polyacrylic Acid as High-Performance Anode for Lithium-Ion Batteries. *ACS Applied Materials & Interfaces* **2016,** *8* (5), 2899-2904.
43. Lopez, J.; Chen, Z.; Wang, C.; Andrews, S. C.; Cui, Y.; Bao, Z., The Effects of Cross-Linking in a Supramolecular Binder on Cycle Life in Silicon Microparticle Anodes. *ACS Applied Materials & Interfaces* **2016,** *8* (3), 2318-2324.
44. Shi, Z.; Jiang, S.; Robertson, L. A.; Zhao, Y.; Sarnello, E.; Li, T.; Chen, W.; Zhang, Z.; Zhang, L., Restorable Neutralization of Poly(acrylic acid) Binders toward Balanced Processing Properties and Cycling Performance for Silicon Anodes in Lithium-Ion Batteries. *ACS Applied Materials & Interfaces* **2020,** *12* (52), 57932-57940.
45. Ward, S. G.; Whitmore, R. L., Studies of the Viscosity and Sedimentation of Suspensions Part 1. - The Viscosity of Suspension of Spherical Particles. *British Journal of Applied Physics* **1950,** *1* (11), 286-290.
46. Olszak-Humienik, M., On the Thermal Stability of Some Ammonium Salts. *Thermochimica Acta* **2001,** *378* (1), 107-112.
47. Oyama, T., Cross-Linked Polymer Synthesis. In *Encyclopedia of Polymeric Nanomaterials*, Kobayashi, S.; Müllen, K., Eds. Springer Berlin Heidelberg: Berlin, Heidelberg, 2021; pp 1-11.
48. Allen, C. L.; Chhatwal, A. R.; Williams, J. M. J., Direct Amide Formation from Unactivated Carboxylic Acids and Amines. *Chemical Communications* **2012,** *48* (5), 666-668.
49. Yang, Y.-H.; Haile, M.; Park, Y. T.; Malek, F. A.; Grunlan, J. C., Super Gas Barrier of All-Polymer Multilayer Thin Films. *Macromolecules* **2011,** *44* (6), 1450-1459.
50. Hsiao, S.-H.; Huang, T.-L., Synthesis and Properties of Novel Polyamides Based on a Benzonorbornane Dietheramine. *Polymer Journal* **2002,** *34* (3), 225-233.
51. Son, B.; Ryou, M.-H.; Choi, J.; Lee, T.; Yu, H. K.; Kim, J. H.; Lee, Y. M., Measurement and Analysis of Adhesion Property of Lithium-Ion Battery Electrodes with SAICAS. *ACS Applied Materials & Interfaces* **2014,** *6* (1), 526-531.
52. Tan, J.; Matz, J.; Dong, P.; Shen, J.; Ye, M., A Growing Appreciation for the Role of LiF in the Solid Electrolyte Interphase. *Advanced Energy Materials* **2021,** *11* (16), 2100046.